Journal of Alloys and Compounds 509 (2011) 5099–5104

Contents lists available at ScienceDirect

Journal of Alloys and Compounds

journal homepage: www.elsevier.com/locate/jallcom

Transparent p-type Cu_xS thin films

P. Parreira [a], G. Lavareda [a], A. Amaral [b], A.M. Botelho do Rego [c], O. Conde [d], J. Valente [a], F. Nunes [a], C. Nunes de Carvalho [a,*]

[a] Materials Science Dept., New University of Lisbon, ICEMS, 2829-516 Caparica, Portugal
[b] Physics Dept., IST, Technical University of Lisbon, ICEMS, 1049-001 Lisboa, Portugal
[c] CQF Molecular and IN, IST, Technical University of Lisbon, 1049-001 Lisboa, Portugal
[d] University of Lisbon, Science Fac., Physics Dept. and ICEMS, 1749-016 Lisboa, Portugal

ARTICLE INFO

Article history:
Received 9 July 2010
Received in revised form 5 January 2011
Accepted 30 January 2011
Available online 1 March 2011

Keywords:
Vacuum evaporation
Cu_xS thin films
p-type conductivity
Mild post-deposition annealing treatments

ABSTRACT

The effect of different mild post-annealing treatments in air, at 270 °C, for 4–6 min, on the optical, electrical, structural and chemical properties of copper sulphide (Cu_xS) thin films deposited at room temperature are investigated. Cu_xS films, 70 nm thick, are deposited on glass substrates by vacuum thermal evaporation from a Cu_2S:S (50:50 wt.%) sulphur rich powder mixture. The as-deposited highly conductive crystalline CuS (covellite) films show high carrier concentration ($\sim 10^{22}$ cm^{-3}), low electrical resistivity ($\sim 10^{-4}$ Ω cm) and inconclusive p-type conduction. After the mild post-annealing, these films display increasing values of resistivity ($\sim 10^{-3}$ to $\sim 10^{-2}$ Ω cm) with annealing time and exhibit conclusive p-type conduction. An increase of copper content in Cu_xS phases towards the semiconductive Cu_2S (chalcocite) compound with annealing time is reported, due to re-evaporation of sulphur from the films. However, the latter stoichiometry was not obtained, which indicates the presence of vacancies in the Cu lattice. In the most resistive films a Cu_2O phase is also observed, diminishing the amount of available copper to combine with sulphur, and therefore the highest values of optical transmittance are reached (65%). The appearance on the surface of amorphous sulphates with annealing time increase is also detected as a consequence of sulphur oxidation and replacement of sulphur with oxygen. All annealed films are copper deficient in regards to the stoichiometric Cu_2S and exhibit stable p-type conductivity.

1. Introduction

Transparent metal oxide (TMO) thin films are a fundamental part of technologies that requires two physical properties usually mutually exclusive: electrical conductivity and optical access in the visible range of the light spectrum. High visible transparency combined with useful electrical conductivity can be achieved by choosing a wide band gap oxide ($Eg \geq 3$ eV) that is rendered conductive through the introduction of native donors (oxygen vacancies) or substitutional higher valence dopants (metal atoms) [1,2]. The most widely used TMOs both in research and industry consist of binary non-stoichiometric compounds such as InO_x, SnO_x and ZnO_x, usually impurity doped with Sn, F and Al, respectively [3–5]. These films are n-type materials with free electron concentration values of the order of 10^{21} cm^{-3} and electrical conductivity that can be as high as 5×10^3 $(\Omega\,\text{cm})^{-1}$, similar to those of typical metals [6,7]. The electrical properties of these transparent oxide materials are highly dependent on deposition and post-deposition processes and can be controlled within an extremely wide range such that they can behave as conductors (TCOs), semiconductors or insulators. Solar cells, thin film transistors, gas sensors and liquid crystal displays are some of the applications where TMO films are frequently used [8–11]. In the late 90s, transparent p-type conductive thin films of copper aluminium oxide ($CuAlO_2$) were reported by Kawazoe et al. [12]. In this context, the development of p–n junctions (basic structure in a variety of devices) exclusively from TMOs became feasible. However, the fabrication of p-type thin films based on wide band gap compounds showed so far that the p-type conductivity is only achieved after post-annealing treatments at high temperature (~450 °C), limiting their field of application [13,14].

Some alternatives to obtain semi-transparent p-type thin films based on narrow band gap materials ($Eg < 3$ eV) have also been reported [15,16]. In the 80s, copper sulphide films (Cu_xS) were extensively studied for solar cell applications (Cu_2S/CdS), being recently reconsidered as a p-type TMO [17,18]. Cu_xS films, 50 nm thick, can reach an average optical transmittance of more than 65% and further reducing of thickness can result in even higher values [19]. They are usually deposited by sputtering or chemical bath techniques, and their p-type conduction is generally attributed to the introduction of native crystalline defects that are easily formed in the non-stoichiometric digenite $Cu_{2-x}S$ phase (free holes from acceptors levels of copper vacancies) [17–20]. However, a detailed

* Corresponding author. Tel.: +351 218419279; fax: +351 218464455/57.
E-mail address: canc@ist.utl.pt (C. Nunes de Carvalho).

0925-8388/$ – see front matter © 2011 Elsevier B.V. All rights reserved.
doi:10.1016/j.jallcom.2011.01.174

Table 1
Evolution of the phase composition of the films, as determined by XRD, with increasing post-annealing time (samples A–E). R: residual amount.

Cu_xS sample phase	A (as-deposited)	B ($t_{ann.}$ = 255 s)	C ($t_{ann.}$ = 285 s)	D ($t_{ann.}$ = 315 s)	E ($t_{ann.}$ = 345 s)
Covellite (CuS)	√				
Digenite (Cu_9S_5)		√	R	√	R
Chalcocite ($Cu_{1.96}S$)			√		√
Cuprite (Cu_2O)				√	√

study of the effect of mild post-annealing treatments in air on the properties of these films is still lacking.

In this paper, we describe the growth of Cu_xS thin films by vacuum thermal evaporation (VTE), on glass substrates, at room temperature. VTE is a unique technique for film growth that does not require chemical reactions taking place in the gas phase and/or at the substrate surface. After mild (270 °C) post-annealing treatments in air, the films show conclusive p-type conductivity with surprising stability. A detailed investigation of the nature and extent of changes in the electrical, optical, surface composition and microstructural properties of Cu_xS films was carried out. The behaviour of the films is explained in terms of their fundamental properties taking into account the mild post deposition annealing treatments.

2. Experimental

Cu_xS thin films were deposited on soda lime and alkali free glass substrates by vacuum thermal evaporation (VTE) at room temperature. After degreasing in proper detergent, rinsing in distilled water and drying in nitrogen gas, the substrates were introduced in the vacuum deposition chamber where a pressure of about 2×10^{-3} Pa is reached. The 2.5 cm × 2.5 cm glass substrates were placed in a substrate holder, at 30 cm above the evaporation crucible. A Balzers BD 482 010 tungsten crucible was used as the powder mixture Cu_2S:S (50:50 wt.%) container. The Cu_xS films were evaporated at very low evaporation rates (0.1–0.3 nm/s) due to different vapour pressures of constituent elements of the mixture, to minimize the deposition of S or Cu rich films during the evaporation process [21]. The evaporation process stopped after a thickness of about 70 nm was reached. For the growth rate and final thickness of the films an Edwards FTM4 thickness monitor was used. The value of the evaporation pressure was about 2×10^{-2} Pa. The post-annealing treatments of the Cu_xS films were performed in the presence of air at 270 °C for an annealing time ranging from 4 to 6 min. A Veeco FPP-5000 four-point probe, capable of determining the type of charge carriers in samples with less than 750 Ω/sq in average, was used for sheet resistance determination. Resistivity, mobility and carrier concentration were measured with a BioRad HL5500 Hall effect system using the Van der Pauw configuration at room temperature with a constant magnetic field (0.5 T). The XPS spectrometer used was a KRATOS XSAM800 operated in the fixed analyser transmission (FAT) mode, with a pass energy of 20 eV, the non-monochromatised Al Kα X-radiation ($h\nu$ = 1486.6 eV) and a power of 120 W (10 mA × 12 kV). Samples were kept on the sample holder by means of a metallic spring and analysed under a typical pressure in the range of 10^{-7} Pa. All sample transfers were made in air. Samples were analysed at room temperature, at take-off angle relative to the surface holder (TOA) of 0°. Spectra were collected and stored in 300 channels with a step of 0.1 eV, and 90 s of acquisition by sweep, using a Sun SPARC Station 4 with Vision software (Kratos). A Shirley background and source satellites were subtracted and curve fitting for component peaks was carried out using Gaussian and Lorentzian products. No flood gun was used for neutralizing charge accumulation. For quantification purposes, sensitivity factors were 0.66 for O 1s, 0.40 for S 2p and 4.45 for Cu $2p_{3/2}$. Phase analysis and crystallinity were studied by grazing incidence X-ray diffraction (GIXRD) at 1° incidence angle to the specimen surface using a Bruker AXS D5000 diffractometer equipped with a Cu Kα X-ray source.

3. Results

The post-annealing conditions of the Cu_xS films will be denoted by samples B–E as identified in Table 1. Annealing treatments with longer periods of time were not considered as the electrical properties of the films were proportionally altered. Post-annealing treatments in vacuum at 10^{-2} mbar were also investigated but did not show any significant changes in the fundamental characteristics of the films. For the sake of convenient comparison, the results obtained from the as-deposited Cu_xS films (sample A) will also be mentioned.

3.1. Surface chemical characterization: XPS analysis

In all the samples the XPS photoelectrons Cu 2p, S 2p and O 1s regions were studied in detail. Some contaminant carbon was also found. S 2p region is shown in Fig. 1. The first striking observation is that for samples C, D, and especially E, an important peak corresponding to sulphate ion develops. Its S $2p_{3/2}$ component is centred at 168.9 ± 0.2 eV. In sample B just an incipient peak appears in the same binding energy region. The peak at lower binding energy has different characteristics from sample to sample: in the A and B samples, three doublets (with a spin–orbit split of 1.6 eV) fit the peak. The S $2p_{3/2}$ component of the first doublet is centred at 161.7 ± 0.1 eV and is assignable to S bound to Cu [22]. For the other two doublets, they are centred at 163.3 ± 0.1 eV and 165.4 ± 0.1 eV. The constancy of the position of the first component for all the samples led us to not correcting binding energies. However, for samples C–E, the first doublet is enough for a good fitting.

The interpretation of this fact needs the observation of Cu 2p regions for the same samples, which are shown in Fig. 2. In the region Cu $2p_{3/2}$, all the samples show, as main component, a peak centred at 932.0 ± 0.2 eV (in fact it is at 931.9 eV for sample A and increases from sample to sample reaching 932.2 eV for samples D

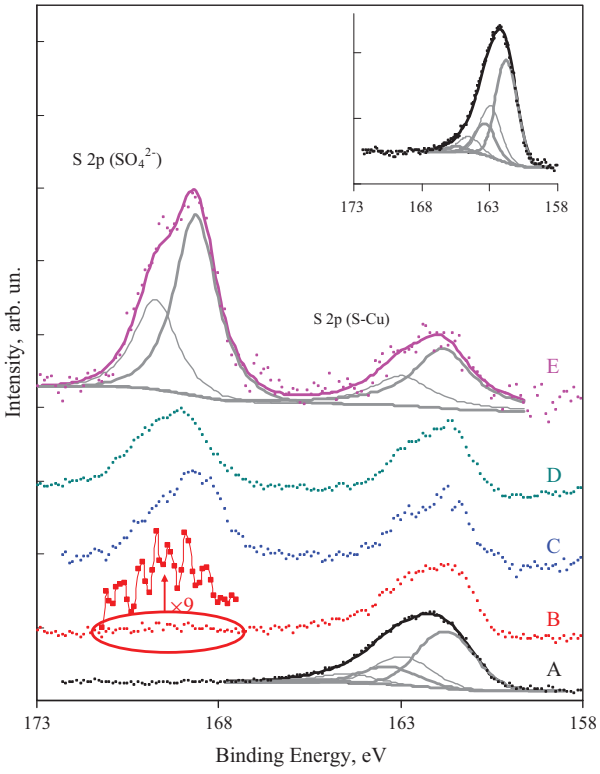

Fig. 1. XPS S 2p region for as-deposited (A) and annealed (B–E) Cu_xS films. Fitted components S $2p_{3/2}$ are represented by thick grey curves and S $2p_{1/2}$ (1.2 eV higher than S $2p_{3/2}$) by thin grey curves. All the spectra were normalized to the S 2p (S–Cu) peak. The inset shows the spectrum of sample A in a compressed scale to display more clearly the less intense doublet hardly seen in the main figure. The region corresponding to sulphate in sample B was zoomed by a factor 9 to show an incipient peak.

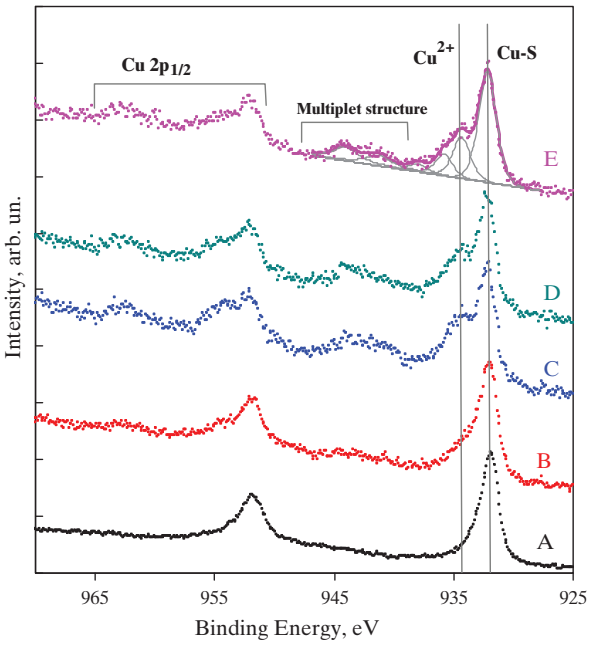

Fig. 2. XPS Cu 2p region for as-deposited (A) and annealed (B–E) Cu_xS films. Just the fitting of the curves A and E are represented for the sake of clarity.

and E) assigned to Cu cuprous form [23,24]. In sample A, a tail towards higher binding energies is fittable with two extra peaks at 933.2 and 934.9 eV, which could suggest the existence of some oxide. But the existence of the oxide would require the existence of O1s photoelectrons at an energy around 530.0 eV. However, this is not observed in sample A, what rules out this hypothesis. These multiple components should be, then, connected with the multiple doublets found in S 2p peak. It is likely that sample A has 3 phases with different conductivities: one conductive and the other ones with an insulating character. The differential charge accumulation should then explain the co-occurrence of three doublets in S 2p and Cu 2p regions. Sample A is the only one where no multiplet structure, due to spin–spin interaction, exists attesting the absence of unpaired electrons. This means that only the species Cu^+ is detected in this sample. In sample B, the same effect occurs but, since an incipient multiplet structure appears, revealing the existence of some Cu with unpaired spins (Cu^{2+}), the extra peaks may also contain a contribution of CuO and $Cu(OH)_2$ or even $CuSO_4$ since S 2p region reveals a tiny amount of sulphur under the form of sulphate ions. In samples C–E, a single phase seems to exist. The main component in Cu $2p_{3/2}$ is assignable to the cuprous form, Cu^+. Since in these samples a large amount of oxygen coexists with sulphur, this Cu^+ may exist under the form of Cu_2O as well as under the form of Cu_xS, with $1 \leq x \leq 2$. In fact, it is reported in the literature that in all the compounds Cu_xS, independently of x, the oxidation state of Cu is unitary [25]. Thence, the smaller components centred at higher binding energies, should correspond to Cu^{2+} under the form of CuO, $Cu(OH)_2$ and/or $CuSO_4$ as referred above for sample B. Accurate quantitative data treatment is not possible, namely for O 1s region, due to some surface contamination developed with the annealing treatment. Since Cu 2p photoelectrons have kinetic energies (~554 eV) much lower than the S 2p ones (~1326 eV), they are much more attenuated by the surface contamination and a distortion of the ratios Cu/S occurs. Anyway, what is observed is that the annealing promotes the increase of the ratio Cu/S and an increase of O/S clearly showing that, besides the oxidation of sulphur, also a replacement of sulphur by oxygen occurs as already revealed by the appearance of oxidized forms in Cu 2p spectra and the development of a multiplet structure. It is worthy to remember that the thickness

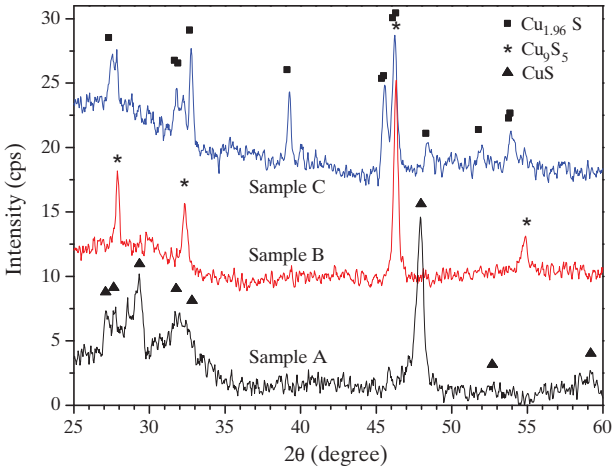

Fig. 3. GIXRD patterns of samples A (as-deposited), B ($t_{ann.}$ = 255 s) and C (t_{ann} = 285 s). For details on the intensity scale refer to the text. Main peaks are labelled according to the JCPDS database.

probed by XPS is around 10 nm (3–5-fold the attenuation length of a given photoelectron), which renders the results presented above valid for a relatively thin surface layer.

3.2. Phase analysis by GIXRD

In contrast to the XPS analysis, X-ray diffraction probes the whole Cu_xS film thickness even when grazing incidence configuration at one-degree incidence angle is employed, as was the case in this study. Indeed, the thickness of a Cu_xS layer contributing to 95% of the diffracted intensity is about 1.67 μm and 1.55 μm for CuS and Cu_2S films respectively, whereas the films analysed by GIXRD are ~70 nm thick. Fig. 3 displays the GIXRD patterns of samples A–C, which were interpreted using the JCPDS database. For comparison, the spectra of samples B and C were shifted along the intensity axis to minimize overlapping of the curves and to allow easier phase identification. All the samples are crystalline although to different extent and different phases are encountered depending on the post-annealing conditions. The reflection peaks shown in spectrum A are mainly due to the covellite (hexagonal) CuS structure while patterns B and C are better indexed using the filecards for digenite (rhombohedral) Cu_9S_5 and chalcocite (tetragonal) $Cu_{1.96}S$, respectively. A residual amount of digenite can still be seen in spectrum C.

When the samples are heat treated in air at 270 °C, they appear to lose sulphur and the stoichiometry becomes Cu_xS with x increasing with annealing time: $x = 1$ at $t = 0$ s (A), $x = 1.8$ at $t = 255$ s (B), $x = 1.96$ at $t = 285$ s (C). As x increases, i.e. The atomic percent of sulphur decreases, new phases are formed corresponding to changes in the solid state that lead to the most stable phase for each composition. The trend observed for the XRD spectra of samples A–C is the expected one from a simple examination of the Cu–S phase diagram as the at.% S in the material becomes lower. Although x approaches the value of two (Cu_2S stoichiometry), the latter is not attained indicating the presence of vacancies in the Cu sub-lattice. In general, the XRD results are in good agreement with the electrical measurements as will be seen later. Based on the previous discussion, it would be expected that with further rising of the post annealing time to 315 s (sample D) and 345 s (sample E) the stoichiometry of the samples would evolve towards the Cu_2S compound. However this is not observed and instead, an oxidation process takes place accompanied by a regression of the stoichiometry. In order to investigate this behaviour the GIXRD patterns of samples D and E are plotted in Fig. 4a and b and compared with those from samples

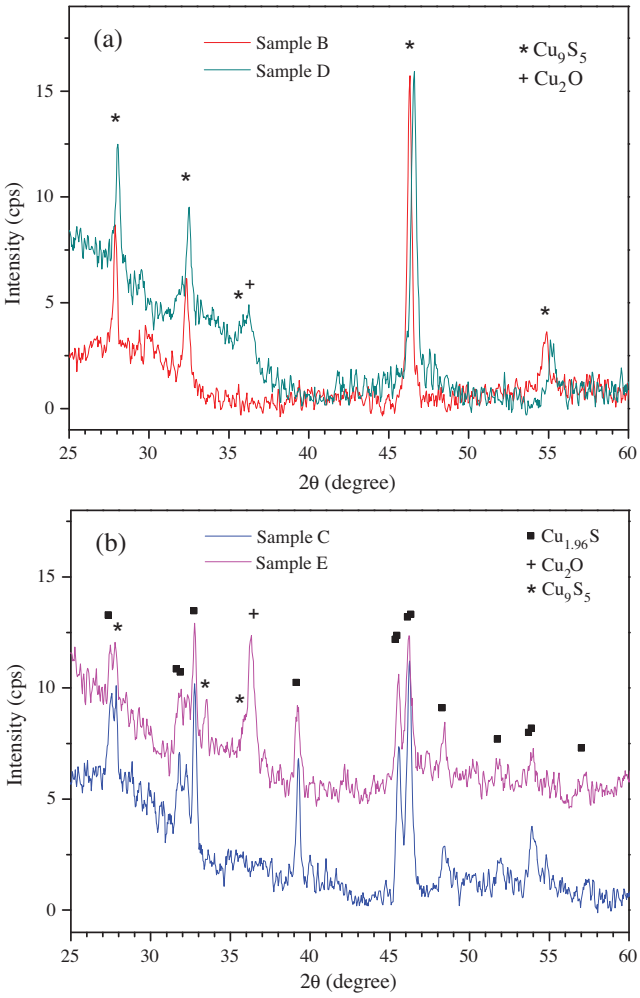

Fig. 4. GIXRD patterns of samples (a) B ($t_{ann.}$ = 255 s) and D ($t_{ann.}$ = 315 s) and (b) C (t_{ann} = 285 s) and E ($t_{ann.}$ = 345 s).

B and C, respectively. Fig. 4a shows that the main peaks characteristic of film B are visible on pattern D which exhibits one more broad peak at $2\theta \sim 36.4^{\circ}$. This latter peak can be assigned to Cu_2O (cuprite) according to the JCPDS filecard no. 5-0667. The peaks on spectrum D are slightly shifted to higher two-theta angle as compared to spectrum B which can be due to a slight different stoichiometry of both samples. A similar evolution is observed by comparing samples C and E in Fig. 4b: sample E consists on the phases already displayed by sample C (chalcocite and residual digenite) and on Cu_2O. These results might be explained by considering that the formation of a Cu oxide phase leaves less copper available to combine with sulphur yielding a Cu_xS phase with x lower than that of the existing phase at the onset of the oxide formation. Accordingly, sample C consists mainly on the chalcocite phase ($x = 1.96$) whereas sample D displays the digenite one ($x = 1.8$) together with cuprite. The evolution from D to E resembles that from B to C. Furthermore, it is clearly seen that the cuprite's peak in E is better defined as compared with the same peak in sample D. The average size of the cuprite crystallites was calculated as 13 and 17 nm respectively for samples D and E, using the Scherrer's equation [26]. This increase, together with the increase of the peak height, indicates that post-annealing time promoted crystallisation and growth of the cuprite nanocrystallites improving the oxidation of the film. Table 1 summarizes the phase analysis previously described. The absence of CuO and $Cu(SO_4)$ in XRD spectra, clearly abundant in XPS spectra, suggests that these two compounds exist either as amorphous phases or, if crystallized,

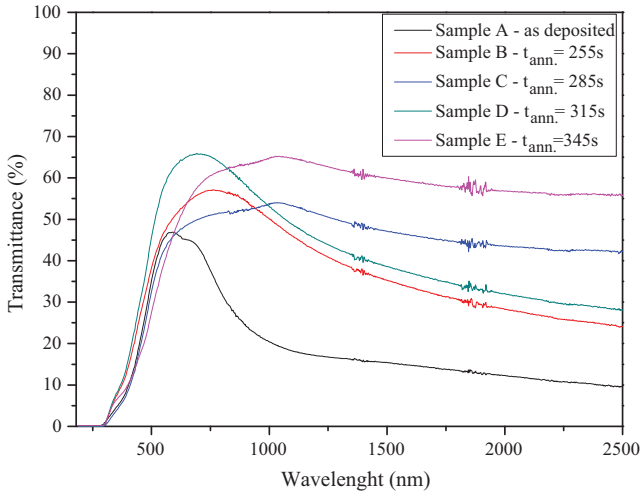

Fig. 5. Comparison of the optical transmittance spectra of as-deposited (A) and annealed (B–E) Cu_xS films, 70 nm thick, deposited by thermal evaporation. Temperature of annealing: 270 °C.

within a thin layer at the surface. In the latter case, the diffracted intensity from those crystalline species would be so weak that it cannot be detected. All the other results are consistent with XPS observations.

3.3. Optical and electrical characterization

The UV–VIS–NIR transmittance spectra for all samples were recorded in the range of $190 \leq \lambda \leq 2500$ nm and are presented in Fig. 5. The optical absorption observed towards shorter wavelengths is usually attributed to transitions from the valence to the conduction band, while the maximum reflectivity is achieved for higher wavelengths governed by free carrier concentration [20]. The total optical transmittance of the films is altered according to the duration of annealing, reaching its maximum (65%) for samples D and E. All samples show a sharp rise in transmittance at the beginning of the visible region but there are clear differences in transmittance towards higher wavelengths. Samples A, B and D show a peaked transmission in the range of 600–800 nm. This peak in transmission is sharp for sample A, becoming smoother for samples B and D. This smoothness evolves towards the increasing in charge carrier concentration. Samples C and E approximately maintain the transmittance throughout the rest of the spectrum, having in common the formation of the chalcocite phase, $Cu_{1.96}S$ (Table 1). Samples also exhibit a decrease in transmission in the NIR region as their phase composition approaches CuS (covellite). Copper sulphide is an indirect narrow-band gap semiconductor with reported band gaps between 1.2 and 2.6 eV [27]. Estimated from the low wavelength region, the Cu_xS films show an increase of optical gap values with annealing time from 1.46 to 1.60 eV, with the exception of sample E whose gap value is 1.27 eV. The optical gap value was inferred from the absorption data by plotting $(\alpha h\nu)^{1/2}$ as a function of $(h\nu)$ (Tauc's plot) where α is the absorption coefficient and $h\nu$ the photon energy, through extrapolation of the linear portion of the plot (Fig. 6). The small optical gap value obtained for sample E may be attributed to the presence of a thin surface layer of CuO, as shown by XPS, whose reported optical gap values are in the range of 1.27–1.51 eV [28]. The change in the optical appearance of the samples with annealing time, from greenish to brownish was also observed. The remarkable absorption in the NIR region of the as-deposited sample is usually related to the high free carrier concentration presented in the material [29].

Table 2
Carrier concentration, Hall mobility, carrier type, Hall coefficient, electrical resistivity and optical gap of as-deposited (A) and annealed (B–E) Cu_xS thin films, 70 nm thick, deposited by thermal evaporation.

Cu_xS sample	Carrier concentration [cm^{-3}]	Hall mobility [$cm^2\,V^{-1}\,s^{-1}$]	Carrier type	Hall coefficient [cm^3/C]	Resistivity [Ω cm]	Optical gap [eV]
A	1.6×10^{22}	1.6	Inconclusive	0.009	1.0×10^{-4}	1.48
B	3.0×10^{21}	1.1	p-type	0.029	1.8×10^{-3}	1.46
C	1.1×10^{21}	1.2	p-type	0.089	4.1×10^{-3}	1.53
D	4.5×10^{20}	2.2	p-type	0.180	5.8×10^{-3}	1.60
E	1.2×10^{20}	3.4	p-type	0.270	1.4×10^{-2}	1.27

Table 2 lists the electrical properties of the Cu_xS films deposited on alkali free glass in the as-deposited and annealed states. Thermoelectric and Hall effect measurements were carried out in all samples in an effort to determine the carrier type. According to the positive sign of the Hall coefficient all the samples are p-type. However, the type of carrier determined by the thermoelectric effect is contradictory for sample A. Ares et al. [30] studied undoped iron disulfide pyrite (FeS_2) films and reported similar discrepancies between the electrical measurements for samples displaying high density of intrinsic lattice point defects, acting as acceptors and donors and thus generating high concentration of both positive and negative carriers.

The set of annealed films were found to be conductors, showing conclusive p-type conduction. The decreasing in mobility verified in sample B in comparison to sample A can be attributed to the initial re-evaporation of sulphur from the films and oxygen incorporation, which occur in the first stages of the annealing process and originate lattice point defects and distortions, more significant for annealing treatments with shorter duration. As annealing time increases, one would expect oxygen atoms to move substitutionally to lattice defect sites (vacancies), leading to an increase of electrical resistivity, associated to a decrease in the high carrier concentration of the films. The recovery of some lattice defects enhanced by annealing processes, leading to an increase in carrier mobility is also verified as shown in Table 2 [31].

4. Discussion

Annealing processes of thin films, in the presence of air, at temperatures higher than the deposition temperature provide oxygen to the film if the film is oxygen deficient. The oxygen incorporation starts at the surface of the film, moving deeper into the film with annealing time. Hence, for conductive thin films, their electrical resistivity increases since the conductive portion starts diminishing. Therefore, the progressive decrease of the electrical conductivity of the Cu_xS films with annealing time can be attributed to oxidation and to the formation of Cu_xS phases towards the semiconducting cupric sulphide phase, Cu_2S. The optical transmittance data for samples A, B and D show a peaked transmission in the range of 600–800 nm. As it was shown, these films consist mainly of Cu_xS phases with the lowest x values (CuS in sample A; $Cu_{1.8}S$ in samples B and D). Therefore, our results corroborate the studies by Grozdanov and Najdoski who reported that this behaviour seems to be associated to the formation of phases towards the CuS phase [20]. On the other hand, an increase of optical gap with annealing time was observed for all samples with the exception of sample E whose gap value is only 1.27 eV. This result can be explained by the different oxidation states of copper that exhibit lower values of optical gap for higher oxidation degrees [32]. The different colours of copper oxides and the sulphates migration to the surface of the films have a significant influence on the change of films colour with annealing time. According to XRD analysis, a promotion of crystallinity with annealing time is also observed, although different phases are found depending on post-annealing conditions. Despite the continuous increase of copper content in the Cu_xS phases and decrease of sulphur with the annealing time, towards the Cu_2S compound, this stoichiometry was not obtained. The oxidation process of Cu, which occurs mainly in samples D and E, diminishes the amount of available copper to combine with sulphur for the Cu_2S phase formation. This regression in stoichiometry causes the maintenance of vacancies in the Cu lattice in all samples, responsible for their p-type conductivity. The presence on the surface of amorphous oxides and sulphates in samples C–E, as shown by the XPS measurements, denotes the oxidation of the surface of the films with annealing time.

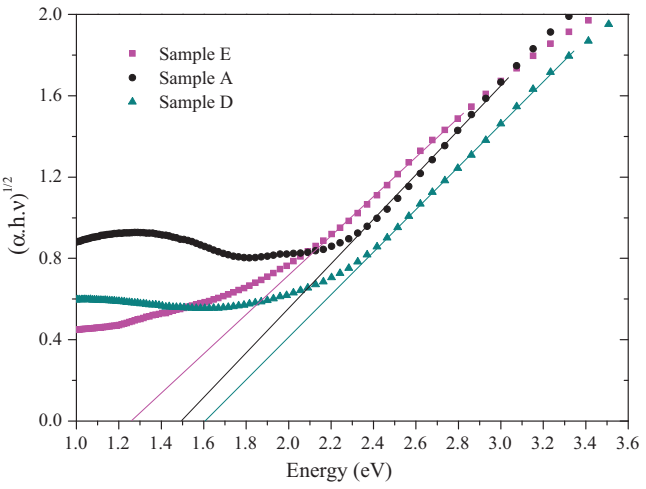

Fig. 6. Variation of $(\alpha h\nu)^{1/2}$ as a function of photon energy for Cu_xS films (samples A, D and E) deposited by thermal evaporation.

5. Conclusions

Cu_xS thin films were deposited by thermal evaporation of a Cu_2S:S (50:50 wt.%) powder mixture on not intentionally heated glass substrates, in vacuum. It was found that annealing treatments in air, during 4–6 min at 270 °C, were the optimum annealing conditions to achieve definitive p-type conduction. The role of oxygen is fundamental as annealing processes in vacuum have no consequences on the properties of the films. For annealed films, the highest carrier concentration obtained was 3.0×10^{21} cm^{-3}, associated with the lowest electrical resistivity of 1.8×10^{-3} Ω cm. Films annealed for the longest period of time displayed a visible transparency of about 65%. According to XRD, all films are polycrystalline and the ratio of copper to sulphur in the films increases with annealing time towards the Cu_2S, due to the decrease of sulphur (re-evaporation of sulphur from the films). However, the latter stoichiometry was not obtained, which indicates the presence of vacancies in the Cu lattice. XPS revealed the presence of surface sulphur and its further oxidation with annealing time. Finally and although much work remains to be accomplished in the optimization and selection of p-type transparent materials, the potential of the Cu_xS thin films as a definitive p-type conductive material with appealing visible transparency properties is outlined in this paper.

With the possibility of controlling the conductivity of these films by adjusting the annealing time, in addition to their p-type conduction stability over time, efforts concerning the integration of these films in devices become a challenge. The field of p-type materials is still at a development stage but the attractiveness of these materials is such that new roads of device research will be open and surely spin-offs into other technology fields will be found.

Acknowledgements

Authors would like to thank Silvia Alessi and Paulo Figueiras without whom this work could have never been done. Authors also wish to thank CENIMAT for Hall measurements. This work was financially supported by the PTDC/EEA-ELC/74334/2006 project.

References

[1] J.L. Vossen, in: G. Hass, M.H. Francombe, R.W. Hoffman (Eds.), Physics of Thin Films, vol. 9, Academic Press, London, UK, 1977.
[2] H.L. Harnagel, A.L. Dawar, A.K. Jain, C. Jagadish, Semiconducting Transparent Thin Films, Institute of Physics Publishing, London, UK, 1995, Ch 3.
[3] I. Hamberg, C.G. Granqvist, J. Appl. Phys. 60 (1986) 123.
[4] S. Major, M.C. Bhatnagar, S. Kumar, K.L. Chopra, J. Vac. Sci. Technol. A 6 (1988) 2415.
[5] S. Masuda, K. Kitamura, Y. Okumura, S. Miyatake, H. Tabata, T. Kawai, J. Appl. Phys. 93 (2003) 1624.
[6] M. Manivvannan, A. Subrahmanyam, J. Phys. D: Appl. Phys. 26 (1993) 151.
[7] R.G. Gordon, MRS Bull. 25 (8) (2000) 52.
[8] V.K. Jain, A.P. Kulshreshtha, Sol. Energy Mater. Sol. Cells 4 (1981) 154.
[9] E. Tokumitsu, M. Senoo, T. Muyasako, Microelectron. Eng. 80 (2005) 305.
[10] M. Suchea, N. Katsarakis, S. Christoulakis, N. Nikolopoulou, G. Kiriakidis, Sens. Actuators B-Chem. 118 (2006) 135.
[11] P.L. Almeida, G. Lavareda, C. Nunes de Carvalho, A. Amaral, M.H. Godinho, M.T. Cidade, J.L. Figueirinhas, Liq. Cryst. 29 (3) (2002) 475.
[12] H. Kawazoe, M. Yasukawa, H. Hyodo, M. Kurita, H. Yanagil, H. Hosono, Nature 389 (1997) 939.
[13] C. Chen, Z. Ji, C. Wang, L. Zhao, Q. Zhou, Mater. Lett. 60 (2006) 3096.
[14] S. Gao, Y. Zhao, P. Gou, N. Chen, Y. Xie, Nanotechnology 14 (2003) 538.
[15] S. Ishizuka, S. Kato, Y. Okamoto, K. Akimoto, J. Cryst. Growth 237/239 (2002) 616.
[16] A.N. Banerjee, S. Kundoo, K.K. Chattopadhyay, Thin Solid Films 440 (2003) 5.
[17] K. Anuar, Z. Zainal, M.Z. Hussein, N. Saravanan, I. Haslina, Sol. Energy Mater. Sol. Cells 73 (2002) 351.
[18] G. Liu, T. Schulmeyer, J. Brotz, A. Klein, W. Jaegermann, Thin Solid Films 431/432 (2003) 477.
[19] K.D. Yuan, J.J. Wu, M.L. Lin, L.L. Zhang, F.F. Xu, L.D. Chen, F.Q. Huang, Appl. Phys. Lett. 93 (2003) 132106.
[20] I. Grozdanov, M. Najdoski, J. Solid State Chem. 114 (1995) 469.
[21] E. Aperathitis, C.G. Scott, J. Phys. Condens. Matter 1 (1999) SB269.
[22] M. Kundu, T. Hasegawa, K. Terabe, M. Aono, J. Appl. Phys. 103 (2008) 073523.
[23] D. Fullston, D. Fornasiero, J. Ralston, Langmuir 15 (1999) 4524.
[24] D. Fullston, D. Fornasiero, J. Ralston, Langmuir 15 (1999) 4530.
[25] J.C.W. Folmer, F. Jellinek, J. Less-Common Metals 76 (1980) 153.
[26] B.D. Cullity, S.R. Stock, Elements of X-ray Diffraction, 3rd ed., Prentice-Hall, Inc., New Jersey, 2001, p. 170.
[27] S.V. Bagul, S.D. Chavhan, R. Sharma, J. Phys. Chem. Solids 68 (2007) 1623.
[28] B. Balamurugan, B.R. Mehta, Thin Solid Films 396 (2001) 90.
[29] H.L. Harnagel, A.L. Dawar, A.K. Jain, C. Jagadish, Semiconducting Transparent Thin Films, Institute of Physics Publishing, London, UK, 1995 (Chapter 4).
[30] J.R. Ares, I.J. Ferrer, C.R. Sánchez, Thin Solid Films 431/432 (2003) 511.
[31] L.I. Maissel in:, L.I. Maissel, R. Glang (Eds.), Handbook of Thin Film Technology, Mc-Graw-Hill Book Company, USA, 1970 (Chapter 13).
[32] G. Papadimitropoulos, N. Vourdas, V. Vamvakas, D. Davazoglou, J. Phys. 10 (2005) 182.